








Diffusion transients in motility-induced phase separation

Shubhadip Nayak ¹, Poulami Bag ¹, Pulak K. Ghosh ^{1,*}, Yunyun Li ^{2,†}, Yuxin Zhou,² Qingqing Yin ²,
Fabio Marchesoni ^{2,3} and Franco Nori ^{4,5}¹Department of Chemistry, Presidency University, Kolkata 700073, India²MOE Key Laboratory of Advanced Micro-Structured Materials, School of Physics Science and Engineering, Tongji University, Shanghai 200092, China³Dipartimento di Fisica, Università di Camerino, I-62032 Camerino, Italy⁴Theoretical Quantum Physics Laboratory, Quantum Computing Center, RIKEN, Wako-shi, Saitama 351-0198, Japan⁵Physics Department, University of Michigan, Ann Arbor, Michigan 48109-1040, USA

(Received 15 August 2024; revised 21 November 2024; accepted 10 January 2025; published 12 February 2025)

We numerically investigate normal diffusion in a two-dimensional athermal suspension of active particles undergoing motility-induced phase separation. The particles are modeled as achiral Janus disks with fixed self-propulsion speed and weakly fluctuating orientation. When plotted versus the overall suspension packing fraction, the relevant diffusion constant traces a hysteresis loop with sharp jumps in correspondence with the binodal and spinodal of the gaseous phase. No hysteresis loop is observed between the spinodal and binodal of the dense phase, as they appear to overlap. Moreover, even under steady-state phase separation, the particle displacement distributions exhibit non-Gaussian normal diffusion with transient fat (thin) tails in the presence (absence) of phase separation.

DOI: [10.1103/PhysRevResearch.7.013153](https://doi.org/10.1103/PhysRevResearch.7.013153)

I. INTRODUCTION

The normal diffusion of an ideal massless Brownian particle is usually associated with the Gaussian distribution of its spatial displacements. However, there are no fundamental reasons why the diffusion of a physical Brownian tracer should be of the Fickian type [1–4]. For instance, displacement distributions in real biophysical systems appear to retain prominent exponential tails, even after the tracer has attained the condition of normal diffusion. Such an effect, often termed non-Gaussian normal diffusion (NGND), disappears only for exceedingly long observation times (possibly inaccessible to real experiments [1]), when the tracer's displacement distribution eventually turns Gaussian, as dictated by the central limit theorem [5]. Persistent diffusive transients of this type have been detected in experimental and numerical setups [6–10]. The signature of NGND, along with a non-Gaussian velocity distribution, has been previously reported in systems with spatial heterogeneity [11–13]. The current interpretation of such diverse NGND manifestations as transient effects postulates the existence of one or more slowly fluctuating processes affecting composition, geometry, and dynamics of the tracer's environment [14–20].

In this paper we report the conspicuous manifestation of NGND in a one-component suspension of identical micro-swimmers undergoing phase separation. The term micro-swimmers refers to either motile micro-organisms, like bacteria, or their synthetic counterparts, typically two-faced colloidal particles [for this reason called Janus particles (JP)], both capable of self-propulsion under nonequilibrium conditions [21–24]. Artificial swimmers are a topic of current research as these can be designed and operated as microrobots for specific applications [25,26].

When investigated collectively, a suspension of active particles may undergo phase separation even in the absence of cohesive forces [27–29]. The ensuing motility-induced phase separation (MIPS) is arguably the simplest nontrivial collective feature that distinguishes active from passive particles [30]. MIPS involves the coexistence of two active phases of different densities, similarly to what happens in a binary fluid mixture below its critical temperature. It occurs as a combined effect of steric interactions and self-propulsion, even in the absence of pair alignment, interactions with solid substrates, or thermal fluctuations [27,28]. Experimental evidence of MIPS has been obtained both in biological and synthetic systems, despite numerous technical difficulties [30].

Inspired by its similarity with equilibrium phase decomposition, much effort has been made to describe MIPS in terms of a nonequilibrium phase transition theory [30–32]. In particular, numerical observations [29] and field theory arguments [33] confirm that the phase diagram of an active suspension exhibits distinct binodal and spinodal lines: in the binodal region enclosed between them, the suspension is in a metastable homogeneous phase, which undergoes slow phase separation through delayed nucleation and fast growth,

*Contact author: pulak.chem@presiuniv.ac.in

†Contact author: yunyunli@tongji.edu.cn

while near and inside the spinodal region it separates by fast coarsening.

Among the quantitative tools employed to numerically characterize MIPS, diffusivity offers arguably the most direct access to the microscopic dynamics underlying phase separation. The asymptotic diffusion constant has been computed as an overall indicator of both gas-liquid [27] and liquid-solid separation [34]. Diffusivity was utilized also to analyze the inner structure of the separating clusters [28].

In this paper we show that diffusion in an athermal active suspension under MIPS may provide a more predictive tool than previously reported. To avoid more complex phase diagrams [35,36], we restrict this report to a two-dimensional (2D) suspension of active hard disks. Such disks undergo normal diffusion no matter what the suspension phase. Upon increasing the suspension packing fraction with uniform initial particle distribution, the diffusion constant exhibits a sharp drop, which we interpret as the gaseous phase spinodal. However, slowly ramping up and down the overall packing fraction, produces a robust hysteresis loop delimited by the binodal and spinodal of the gaseous phase. Vice versa, within our numerical accuracy, the binodal region of the dense phase appears to collapse, so that no hysteretic diffusion loop was observed. Moreover, in the presence of MIPS, the corresponding particle displacement distributions are leptokurtic for extended time transients (i.e., tend to zero slower than a Gaussian function), a clear-cut NGND manifestation.

II. MODEL

We simulated a two-dimensional suspension of N identical achiral active JP's modeled as disks of radius r_0 and constant self-propulsion speed v_0 , in a square box of size L with periodic boundary conditions. The dynamics of a single JP of coordinates $\mathbf{r} = (x, y)$ obeys the simple Langevin equations,

$$\dot{\mathbf{r}} = \mathbf{v}_0, \quad \dot{\theta} = \sqrt{D_\theta} \xi_\theta(t). \quad (1)$$

Here the orientation of the self-propulsion vector $\mathbf{v}_0 = v_0(\cos\theta, \sin\theta)$, measured with respect to the longitudinal x axis, fluctuates subjected to the stationary, delta-correlated noise source $\xi_\theta(t)$, with $\langle \xi_\theta(t)\xi_\theta(0) \rangle = 2\delta(t)$. Following Ref. [27], the suspension is assumed to be athermal, that is, we neglect thermal fluctuations against the angular noise intrinsic to the self-propulsion mechanism [37,38]. The reciprocal of D_θ defines the correlation time, τ_θ , and the persistence length $l_\theta = v_0/D_\theta$ of a free self-propelled JP. For $t \gg \tau_\theta$, a free JP would undergo normal diffusion with diffusion constant $D_s = v_0^2/2D_\theta$, but non-Gaussian statistics.

At short distances the disks repel each other via the pair potential [39],

$$V_{ij} = 4\epsilon[(\sigma/r_{ij})^{12} - (\sigma/r_{ij})^6 + 1/4] \quad \text{if } r_{ij} \leq r_m \\ = 0 \quad \text{otherwise,} \quad (2)$$

where $i, j = 1, \dots, N$ are the pair labels, $r_m = 2^{1/6}\sigma$, $\epsilon = 1$, and $\sigma = 2r_0$ represents the ‘‘nominal’’ disk diameter. The steric interactions of Eq. (2) are not corrected for hydrodynamic effects [23,40]. To save computer time, the suspension packing fraction, $\bar{\phi} = \pi r_0^2 N/L^2$, was varied by changing the box size, while keeping the number and radius of the

disks fixed. The stochastic differential Eqs. (1) were integrated numerically by means of a standard Euler-Maruyama scheme [41].

As illustrated in Secs. III and IV the MIPS phenomenon was readily reproduced at fixed v_0 by increasing $\bar{\phi}$. Upon approaching the MIPS onset at $\bar{\phi} = \bar{\phi}_*$, short-lived aggregates in the homogeneous phase anticipate the separation into a gaseous (or dilute) and a dense phase: for $\bar{\phi} < 0.5$ ($\bar{\phi} > 0.5$) a single large cluster (cavity) forms in the simulation box. Most notably, tagged particles diffuse homogeneously across the simulation box also in the presence of phase separation, i.e., for $\bar{\phi} > \bar{\phi}_*$, no matter what the cluster size.

A JP of speed v_0 and persistence time τ_θ is characterized by a mean ballistic path, or persistence length, $l_\theta = v_0\tau_\theta$. This dynamical length should be compared with the other characteristic length scales in the homogeneous phase. As known from the classical kinetic gas theory, they are (i) the average particle distance, $l_L = \sqrt{L^2/N}$, and (ii) the mean-free path between pair collisions, $l_c = L^2/N\sigma$. We ignore here the particle diameter, $\sigma = 2r_0$, as we kept it comparatively small throughout our numerical investigation. When expressed in terms of the overall suspension packing fraction $\bar{\phi}$, the lengths above read respectively

$$l_L = \sqrt{\pi r_0^2/\bar{\phi}} \quad \text{and} \quad l_c = \pi r_0/2\bar{\phi}.$$

This implies that, if we keep $\bar{\phi}$ fixed and vary the particle number N , the ratios l_L/l_θ and l_c/l_θ do not change.

Being MIPS a collisional mechanism [42], we limited our investigation to suspension densities with $l_c \geq l_L$, that is, on $\bar{\phi}$ values not exceeding the close-collision packing fraction $\phi_{cc} = \pi/4$, an upper bound slightly smaller than the close packing fraction $\phi_{cp} = 2\sqrt{3}/\pi$, often mentioned in the literature.

III. PARTICLE SELF-DIFFUSION AND MOTILITY-INDUCED PHASE SEPARATION

To characterize the particle diffusivity in the suspension, we monitored two quantities. (i) The first is the particle mean-square displacement (MSD), say, in the x direction, $\langle \Delta x^2(t) \rangle$, with $\Delta x(t) = x(t) - x(0)$. In view of the established ergodic character of the diffusive process, ensemble averages, $\langle \dots \rangle$, were taken over all N suspension particles [40]. (ii) The second quantity is the probability density function (pdf) of the particle displacement Δx at time t , $P(\Delta x, t)$. Both quantities were computed after the suspension had reached an apparently steady-state configuration. Note that $P(\Delta x, t)$ displays a small periodic oscillatory pattern due to the periodic boundary conditions applied in our simulation. However, this effect does not affect the findings reported in this paper.

Our numerical data [Fig. 1(a)] clearly show that for sufficiently large observation times, typically $t \gg \tau_\theta$, the MSD grows according to the Stokes-Einstein law, $\langle \Delta x^2(t) \rangle = 2Dt$, which defines the particle self-diffusion constant in the suspension, D . This constant is a function of $\bar{\phi}$: A sudden diffusivity drop marks phase separation. This MIPS signature is sharp enough to determine $\bar{\phi}_*$ as a function of v_0 . As apparent in Figs. 1(b), 1(c), 2(c), and 2(d), no MIPS occurs for v_0 below a critical value, $v_0^* \simeq 0.25$, while for $v_0 > v_0^*$ the

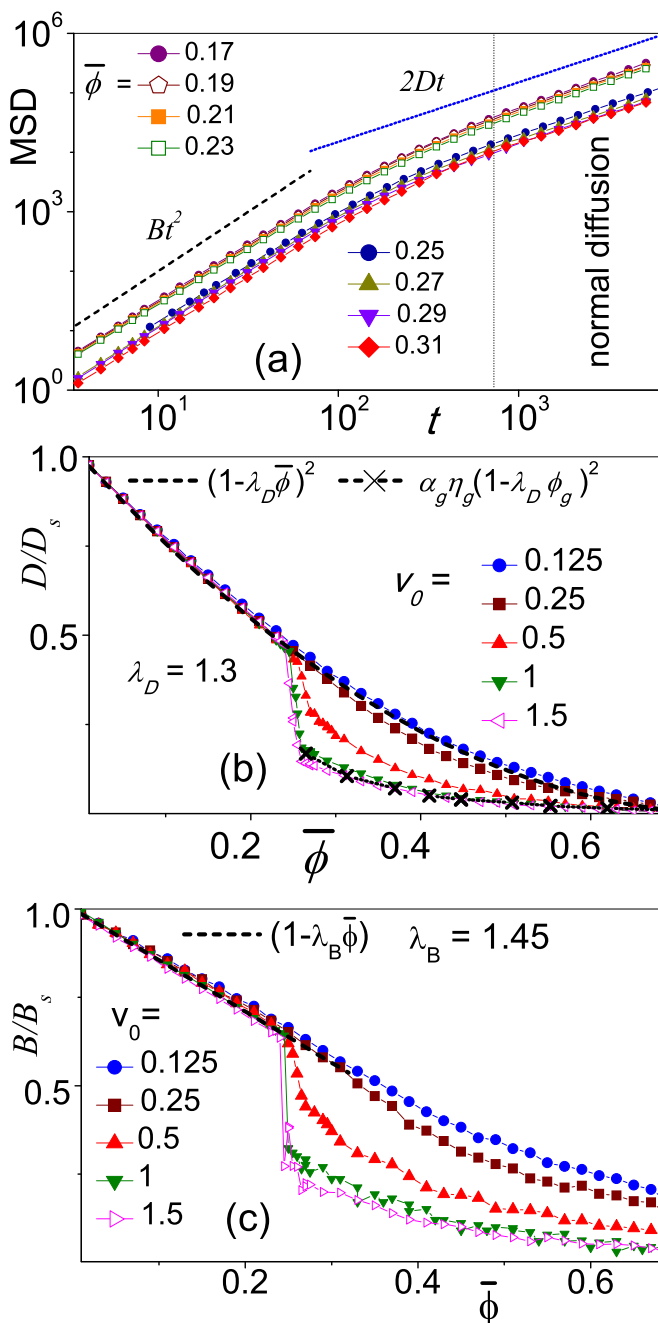


FIG. 1. Particle mean-square displacement (MSD) in a suspensions of N active JP's of radius $r_0 = 1$ and persistence time $\tau_\theta = 100$; $N = 9, 120$. Packing fraction $\bar{\phi}$ was varied by tuning simulation box size at fixed N . If not stated otherwise, the suspension was initially randomly uniform. (a) MSD, $\langle \Delta x^2(t) \rangle$, vs t for $v_0 = 1$ and different $\bar{\phi}$. The short-time ballistic and the asymptotic diffusive branches are fitted respectively by quadratic, Bt^2 , and linear, $2Dt$, functions. The fitting parameters D (in units of $D_s = v_0^2/2D_\theta$) are plotted in (b) vs $\bar{\phi}$. The fitting parameters B (in units of $B_s = v_0^2/2$) vs $\bar{\phi}$ with different v_0 (see legend) are plotted in (c). The dashed lines in (b) and (c) depicting the $\bar{\phi}$ dependence of D/D_s and B/B_s (for $v_0 = 1$) are fitted by the functions in the legends. Crosses in (b) display Eq. (4) [see text for details].

dependence of $\bar{\phi}_*$ on v_0 is rather weak. Similarly, Fig. 2(d) shows that for a given v_0 there exists an upper bound for the

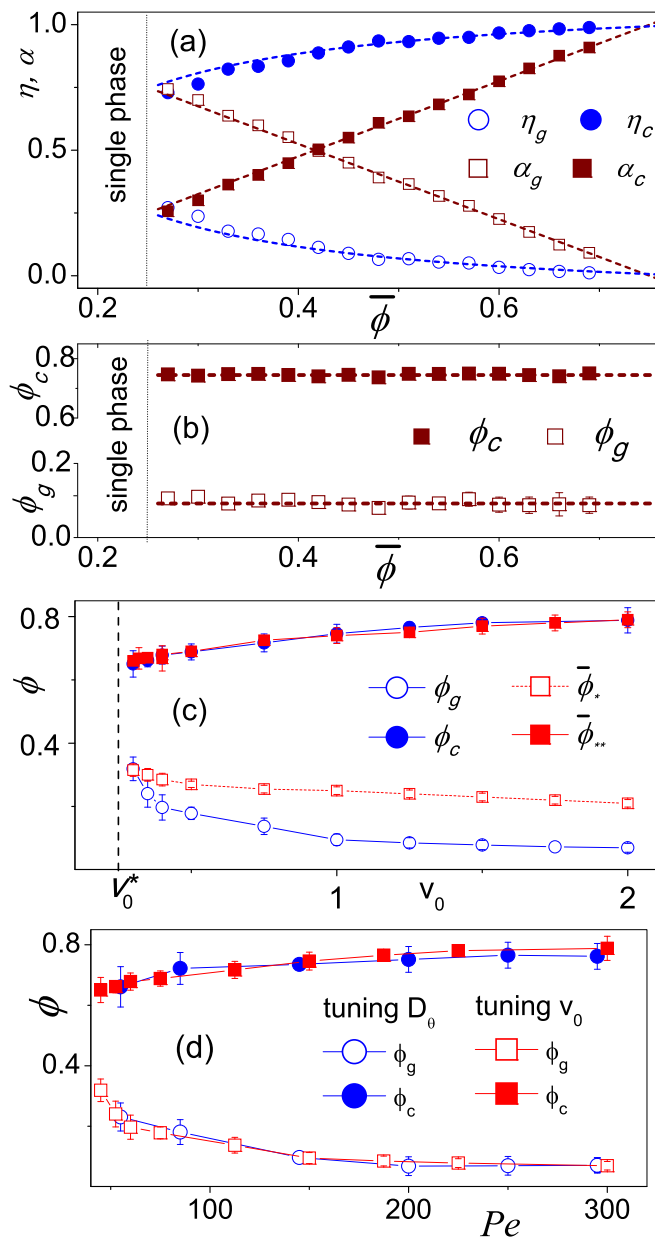


FIG. 2. Gaseous and dense phases (denoted respectively by the indices $i = g, c$): $\bar{\phi}$ dependence of (a) the phase number, η_i , and volume, α_i , fractions and (b) the phase packing fractions, ϕ_i , for $N = 10^4$, $v_0 = 1$, $\tau_\theta = 100$, and random uniform initial conditions. As a consistency test, we fitted the data for α_i and ϕ_i with straight lines [dashed lines respectively in (a) and (b)] and made use of the identity $\phi_i = \bar{\phi}\eta_i/\alpha_i$ (see text) to reproduce the $\bar{\phi}$ dependence of η_i in (a). Fitting functions: $\alpha_c = 1.5\bar{\phi} - 0.14$, $\phi_c = 0.75$, and $\phi_g = 0.09$. Recall that $\alpha_g + \alpha_c = 1$ and $\eta_g + \eta_c = 1$. (c) Cluster, ϕ_c , gaseous phase, ϕ_g , and MIPS onset, $\bar{\phi}_*$ and $\bar{\phi}_{**}$, packing fractions vs v_0 for $\bar{\phi} = 0.45$. For $v_0 < v_0^*$ MIPS never occurs, while for $v_0 > v_0^*$ our data suggest that $\phi_g^{(s)} + \phi_c^{(s)} = 1$. (d) Gaseous and cluster phase binodal, ϕ_g and ϕ_c , vs $Pe = 3v_0/(2r_0D_\theta)$ for $N = 9, 120$, $v_0 = 1$ (blue symbols), and $D_\theta = 10^{-2}$ (red symbols).

angular diffusion constant D_θ , above which MIPS does not occur.

In the homogeneous phase, the fitting ballistic, B , and diffusion, D , constants of Fig. 1(a) appear to slowly decrease

with increasing $\bar{\phi}$ up to the MIPS onset, $\bar{\phi} = \bar{\phi}_*$. Standard stoichiometric arguments suggest polynomial fitting laws,

$$D = D_s(1 - \lambda_D \bar{\phi})^2 \quad \text{and} \quad B = B_s(1 - \lambda_B \bar{\phi}), \quad (3)$$

with $D_s = v_0^2 \tau_\theta / 2$ and $B_s = v_0^2 / 2$. Both fitting parameters λ_B [in Fig. 1(c)] and λ_D [in Fig. 1(b)] are larger than the reciprocal of the close-collisional packing fraction, $\phi_{cp} = \pi/4$, introduced in Sec. II, and $\lambda_B > \lambda_D$. We attribute this behavior to the residual softness of the repulsive WCA potential. Similarly to the diffusivity curves, MIPS drops of the curves $B(\bar{\phi})$ are apparent, in quantitative agreement with the existence of a critical value v_0^* , below which MIPS is ruled out [see Figs. 2(c) and 2(d)]. These findings are consistent with the conventional analysis of the stationary local packing fraction distribution.

To analyze the tails of $D(\bar{\phi})$ for $\bar{\phi} > \bar{\phi}_*$, we had recourse to the two-phase characterization of Figs. 2(a) and 2(b) (also for $v_0 = 1$). After exceedingly long simulation runs, $t = 10^5$, the dense and dilute phases of the suspension appear to be well separated. We computed the volume, α_i , and number, η_i , fractions of both phases and the resulting phase packing fractions, ϕ_i ($i = g, c$ denoting, respectively, the gaseous and the dense phases). To this purpose we first computed the corresponding phase densities ρ_i , by selecting rectangular regions (as large as possible) within either phases and then counting particles in there. This procedure was repeated 10 times for different “trajectories,” namely initial configurations and random number sequences. This way we estimated the phase mean densities as well as their standard deviations (under the simplifying assumption that both phases were homogeneous). Finally, we computed the phase areas, A_i , by imposing the two normalization conditions $\rho_c A_c + \rho_g A_g = N$ and $A_c + A_g = L^2$.

By definition, $\phi_i = \bar{\phi} \eta_i / \alpha_i$, as numerically checked in Fig. 2(a). The densities of the two phases are confirmed to be independent of $\bar{\phi}$ [28]. On neglecting the contribution from the particles trapped in the cluster, the self-diffusion constant for $\bar{\phi} > \bar{\phi}_*$ can be approximated to

$$D_{\text{MIPS}}(\bar{\phi}) = \alpha_g \eta_g D_s (1 - \lambda_D \phi_g)^2. \quad (4)$$

Here, we made use of the fact that the gaseous phase represents a fraction η_g of the suspension and behaves as a homogeneous phase with low packing fraction ϕ_g and fractional volume α_g . A comparison with the actual D data for $v_0 = 1$ is displayed in Fig. 1(b).

IV. HYSTERESIS LOOPS AND BINODAL POINTS

In order to clarify the meaning of $\bar{\phi}_*$, we notice that for $\bar{\phi} > \bar{\phi}_*$ the cluster volume fraction α_c grows linearly with the overall packing fraction. Our simulation results for $\alpha_c(\bar{\phi})$ fit well (within numerical error) with the following empirical relation,

$$\alpha_c(\bar{\phi}) = (\bar{\phi} - \phi_g) / (\phi_c - \phi_g), \quad (5)$$

where $\phi_c(\phi_g)$ is the packing fraction of a dense (dilute) one-phase suspension, i.e., for $\alpha_c = 1$ [$\alpha_c = 0$, out of range in Fig. 2(a)]. This simple graphical construction allows one to quickly determine both binodal points, ϕ_g and ϕ_c , at fixed v_0 , in good agreement with the simulation of Fig. 2(b). Their dependence on v_0 , displayed in Fig. 2(c) for $\bar{\phi} = 0.45$, qualitatively agrees with the simulation results of Refs. [28,29].

Note that we never increased v_0 large enough to explore either the full phase diagram [43,44] and/or the reentrant MIPS [45]. Furthermore, the spinodal curves displayed in Fig. 2(c) remain unchanged as the system size increases up to $N = 50\,000$. For this large system size, we conducted simulations with a duration of $t = 20\,000$. However, these results may vary for significantly larger system sizes and longer simulation runs, which lie beyond our computational capabilities.

A. The gaseous phase spinodal and binodal

In contrast with Refs. [27,28], by starting with a uniform particle distribution we never observed MIPS in the range $\bar{\phi} \in [\phi_g, \bar{\phi}_*]$, regardless of the (accessible) running time. The outcome changed when we slowly increased (decreased) $\bar{\phi}$ over time. We did so by keeping N fixed and decreasing (increasing) L stepwise after a fixed long running time Δt (typically $\Delta t = 5 \times 10^4$). Upon varying L , we rescaled the suspension configuration accordingly. This produced the hysteresis loops of Fig. 3(a), which, for large N , approach the ideal loop obtained by connecting the fitting functions of D vs $\bar{\phi}$ in Fig. 1(b) [also see Eqs. (3) and (4)]. On increasing $\bar{\phi}$, MIPS occurs, as anticipated above, at $\bar{\phi}_*$ (signaled by a D drop), but upon decreasing $\bar{\phi}$ it only disappears for $\bar{\phi} \gtrsim \phi_g$ (signaled by a fast D rise).

The reference or ideal hysteresis loop in Fig. 3(a) (blue dashed lines) was obtained by extending the $\bar{\phi}$ -function D_{MIPS} [see Eq. (4)] to $\bar{\phi}$ values below the MIPS threshold $\bar{\phi}_*$. On making use of Eq. (5), the MIPS branch of the loop can be written as

$$\frac{D_{\text{MIPS}}}{D_s} = \left(\frac{\phi_c - \bar{\phi}}{\phi_c - \phi_g} \right)^2 \frac{\phi_g}{\bar{\phi}} (1 - \lambda_D \phi_g)^2, \quad (6)$$

hence $D_{\text{MIPS}}(\phi_g) = D(\phi_c)$.

To check robustness of the hysteretic effect toward translational noises, we simulate Eq. (1) after adding a 2D translational Gaussian noise term with strength D_0 , $\xi(t) = (\xi_x(t), \xi_y(t))$ with $\langle \xi_i(t) \rangle = 0$ and $\langle \xi_i(t) \xi_j(0) \rangle = 2D_0 \delta(t)$ for $i, j = x, y$, to Eq. (1). The hysteresis loop of Fig. 3(a) there turned out to be quite robust; indeed, it appeared to vanish only for D_0 of the order of D_s . Vice versa, its area may be quite sensitive to the suspension size, N .

Recall that our hysteresis protocol $\bar{\phi}$ was increased/decreased stepwise at regular time intervals Δt . Of course, we cannot rule out the possibility that the resulting hysteresis loop shrinks and finally disappears for exceedingly large Δt (in any case, well beyond our computing capabilities). Similar remarks apply to even simpler dynamically bistable systems, such as the motility of a weakly damped, driven Brownian particle confined to a one-dimensional washboard potential [46]. For the suspension of Fig. 3(a), we repeatedly looped $\bar{\phi}$ in the range (0.05, 0.30), that is, across the relevant binodal and spinodal of the gaseous phase.

As we verified that the hysteretic effect is robust toward translational noises, it has also been noticed that hysteresis loops become sharper upon increasing the suspension size, N , and the observation time, t . In conclusion, accurate data for the $D(\bar{\phi})$ hysteresis loop suffice to self-consistently characterize the gaseous binodal region at fixed v_0 . Further, the

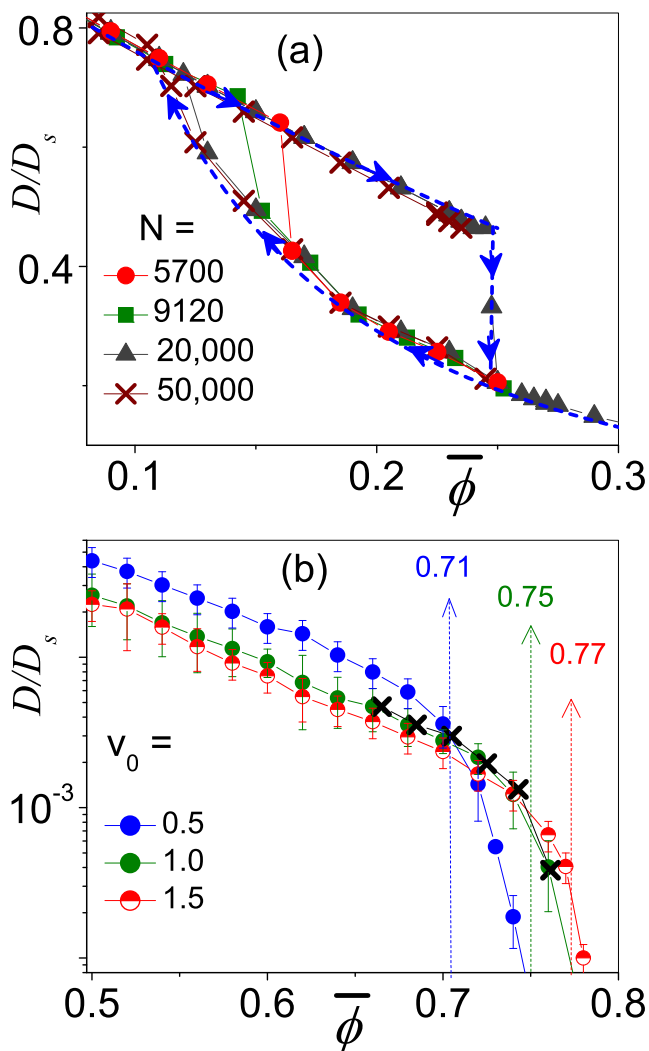


FIG. 3. (a) Hysteresis loop obtained by slowly ramping $\bar{\phi}$ up and down across the gaseous binodal-spinodal range for $v_0 = 1$ with different N (see legends). The reference hysteresis loop (dashed blue curve) has been closed by extending the lower fitting curve, $D_{\text{MIPS}}(\bar{\phi})$, in Fig. 1(b) down to $\bar{\phi} = \bar{\phi}_g$. (b) D vs $\bar{\phi}$ in the upper binodal region for different v_0 and $N = 20,000$. For $v_0 = 1$, D was determined as in (a), by ramping $\bar{\phi}$ up (dots) and down (crosses); no hysteresis loop was detected, as the upper binodal region appears to collapse.

persistence of uniformly distributed short-time aggregates in the suspensions with $\bar{\phi} \lesssim \bar{\phi}_*$, suggests interpreting $\bar{\phi}_*$ as the gaseous phase spinodal [28,29], $\bar{\phi}_* = \phi_g^{(s)}$.

B. The cluster spinodal and binodal

A similar approach was adopted by simulating initially homogeneous, dense suspensions and decreasing $\bar{\phi}$ below ϕ_c : at a sufficiently low value of the overall packing fraction, $\bar{\phi} = \bar{\phi}_{**} < \phi_c$, the dense suspension developed coalescing gaseous bubbles. Therefore, the curve $\bar{\phi}_{**}$ versus v_0 displayed in Fig. 2(c) is our best estimate of the cluster spinodal, $\phi_c^{(s)}$. As illustrated in Fig. 3(b), at $\bar{\phi} = \phi_c^{(s)}$, the curves D versus $\bar{\phi}$ exhibit a second drop, though not as sharp as at $\bar{\phi} = \phi_g^{(s)}$, but no hysteretic loop. In fact, cluster binodal and spinodal curves

run so close to one another that we could hardly separate them; the upper binodal region appears to collapse (see Ref. [33] for an analytical treatment). Remarkably enough, our numerical data suggest that $\phi_g^{(s)} + \phi_c^{(s)} = 1$. As v_0 approaches v_0^* (from above), both upper and lower pairs of binodal and spinodal curves overlap.

V. NON-GAUSSIAN NORMAL DIFFUSION AND PHASE SEPARATION

So far we have characterized MIPS in terms of particle self-diffusion under the condition of normal diffusion, i.e., for $t \gg \tau_\theta$. The question now arises whether this criterion suffices to define the relaxational properties of the suspension steady-state. To address this issue we computed the particle displacement distributions, $P(\Delta x, t)$, at increasing time intervals t . Examples are reported in Fig. 4, for noninteracting particles [panel (a)], interacting particles with $\bar{\phi} < \bar{\phi}_*$ [panels (b) and (c)] and $\bar{\phi} > \bar{\phi}_*$ [panel (d)]. In all cases, the displacement pdf's keep changing over time even in the normal diffusion regime of Fig. 1(a), which implies that the particle dynamics in large steady-state active suspensions involves long transients, largely ignored in previous investigations. Stationary Gaussian distributions were obtained, indeed, but only for exceedingly long simulation runs. More remarkably, when plotted versus Δx in the normal diffusion regime, the transient Δx pdfs are platykurtic in the homogeneous phase and leptokurtic under phase separation. With this notation we mean that, in the presence (absence) of phase separation, the Δx pdf's have thinner (fatter) tails than the corresponding asymptotic Gaussian distributions. It should be remarked that the transition from platy- to leptokurtic transients is as not much a signature of the gaseous spinodal crossing, $\phi_g^{(s)}$, as a property of the cluster phase itself. Indeed, it has been observed all along the lower (MIPS) branch of the hysteresis loop for $\phi_g < \bar{\phi} < \phi_g^{(s)}$ [compare Figs. 4(b) and 4(c)].

A. Heuristic fitting function bridging Gaussian and non-Gaussian displacement distribution

For a more quantitative analysis of the transient Δx distributions, we had recourse to the heuristic fitting function, $P(\Delta x/\sqrt{t}, \beta)$, first introduced in Ref. [20] to bridge Gauss ($\beta = 2$) and Laplace (i.e., exponential, $\beta = 1$) pdfs with the same MSD, $2Dt$, namely,

$$P_G(\Delta x, t; D) = \frac{1}{\sqrt{4\pi Dt}} \exp\left[-\frac{\Delta x^2}{4Dt}\right] \text{ and}$$

$$P_L(\Delta x, t; D) = \frac{1}{\sqrt{Dt}} \exp\left[-\frac{|\Delta x|}{\sqrt{Dt}}\right].$$

In contrast to the diffusing diffusivity model [14], where the limiting Laplace and Gaussian distributions are functions of the sole diffusion constant D , a more realistic fitting procedure needs at least one additional t -dependent parameter, β , to capture the transient character of the displacement pdfs. To this purpose, in Ref. [20], we started from the compressed exponential function

$$p(\delta_t) = p_0 \exp[-(\delta_t/\delta_0)^\beta], \quad (7)$$

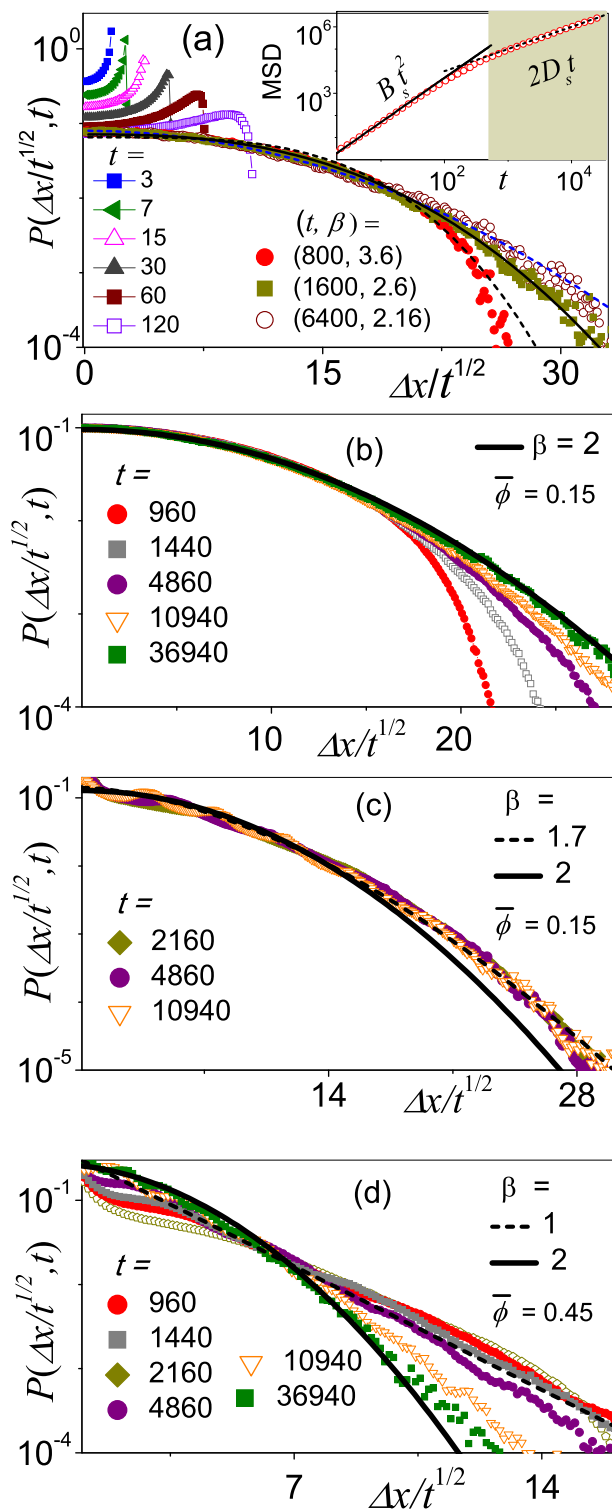


FIG. 4. Non-Gaussian normal diffusion as a MIPS signature. (a) Particle diffusion in an active suspension of non-interacting JPs, $\epsilon = 0$, at different times t (see legend). The transient (platykurtic) fitting curves, $P(\Delta x/\sqrt{t}, \beta)$ with $\beta = 3.6, 2.6,$ and 2.16 , appear to fit well the numerical data. As to be expected, the fitting parameters B and D in the inset coincide with $B_s = v_0^2/2$ and $D_s = v_0^2/2D_\theta$. (b) Δx pdf for increasing t values and $\bar{\phi} > \bar{\phi}_*$ (see legend); the Gaussian ($\beta = 2$, solid) and Laplace distributions ($\beta = 1$, dashed) for the D value fitting the corresponding data in Fig. 1(a) are drawn for reference. In (c) and (d), Δx pdf's are displayed for suspension configurations with the same $\bar{\phi}$, but resting respectively on the up-

where $\delta_t = \Delta x/\sqrt{t}$ and $\beta \geq 1$. The scaling factor δ_0 and the normalization constant p_0 were computed by imposing the conditions

$$\int_0^\infty p(\delta_t) d\delta_t = 1, \quad \int_0^\infty \delta_t^2 p(\delta_t) d\delta_t = 2D \quad (8)$$

to obtain the one-parameter *ad hoc* fitting function

$$P(\delta_t, \beta) = \frac{\beta}{\Gamma(\frac{1}{\beta})^{\frac{1}{\beta}}} \left[\frac{\Gamma(\frac{3}{\beta})}{2D} \right]^{\frac{1}{\beta}} \exp \left[- \left(\frac{\delta_t^2}{2D} \frac{\Gamma(\frac{3}{\beta})}{\Gamma(\frac{1}{\beta})} \right)^{\frac{\beta}{2}} \right]. \quad (9)$$

This is the definition of the fitting functions, $P(\Delta x/\sqrt{t}, \beta)$, plotted in Fig. 4. The fitting parameter β is allowed to vary with t ; it assumes values in the range $1 \leq \beta \leq 2$ for leptokurtic distributions (positive excess kurtosis) and $\beta \geq 2$ for platykurtic distributions (negative excess kurtosis).

The β values displayed in Fig. 5 have been generated from Eq. (9) by setting D equal to the diffusion constants that best fitted the large- t diffusion data in Fig. 1(b) and then computing β to get the best fit of the $\Delta x/\sqrt{t}$ distributions at different t . The numerical transients of a suspension of non-interacting active particles for $t \gtrsim \tau_\theta$, displayed here in Fig. 4(a), are well reproduced by this fitting function. The $P(\Delta x/\sqrt{t}, \beta)$ spikes at short times, $t < \tau_\theta$, are centered around $v_0\sqrt{t}$, as expected in the ballistic regime.

We recall that when taking into account steric effects, all distributions $P(\Delta x, t)$ were computed after the active suspension had reached its stationary state. This means that for $\bar{\phi} > \bar{\phi}_*$ we started counting t only after MIPS had occurred. Leptokurtic transients with t -dependent β are a defining MIPS property, as proven by the fact that NGND was observed along the entire lower branch of the hysteresis loops of Fig. 3(a). An example is illustrated in Figs. 4(b) and 4(c).

The transient character of the Δx distributions was thus quantified by the t -dependent fitting parameter β . In Figs. 5(a) and 5(b) we display β vs t for $v_0 = 1$, randomly uniform initial conditions and increasing values of $\bar{\phi}$. All curves approach the horizontal asymptote, $\beta = 2$, as expected; more importantly, they do so from above for $\bar{\phi} < \bar{\phi}_*$ and from below for $\bar{\phi} > \bar{\phi}_*$. The transition from platy- to leptokurtic transient pdfs is the sharpest at short normal diffusion times. This property provides an alternative but consistent signature of the MIPS threshold ($\bar{\phi}_* = 0.245 \pm 0.005$ for $v_0 = 1$). It should be remarked that the transition from platy- to leptokurtic transients is not much a signature of the gaseous phase spinodal, $\bar{\phi} = \phi_g^{(s)}$, as a property of the cluster phase itself. Indeed, it has been observed also along the lower (MIPS) branch of the hysteresis loop for $\phi_g < \bar{\phi} < \phi_g^{(s)}$.

The transient displacement distributions, $P(\Delta x, t)$, in a low-density active suspension are governed solely by diffusion in a homogeneous phase, whence their platykurtic character [20]. Vice versa, under phase separation the JPs tend to cluster in compact structures made of hexatic domains

per ($\beta > 2$) and lower ($\beta < 2$) branches of the hysteresis loop of Fig. 3(a). Other simulation parameters are $\tau_\theta = 100$, $v_0 = 1$, and $N = 9120$. The estimated NGND transient time is $\tau_{\text{NGND}} \sim 7.5 \times 10^5$ (see text).

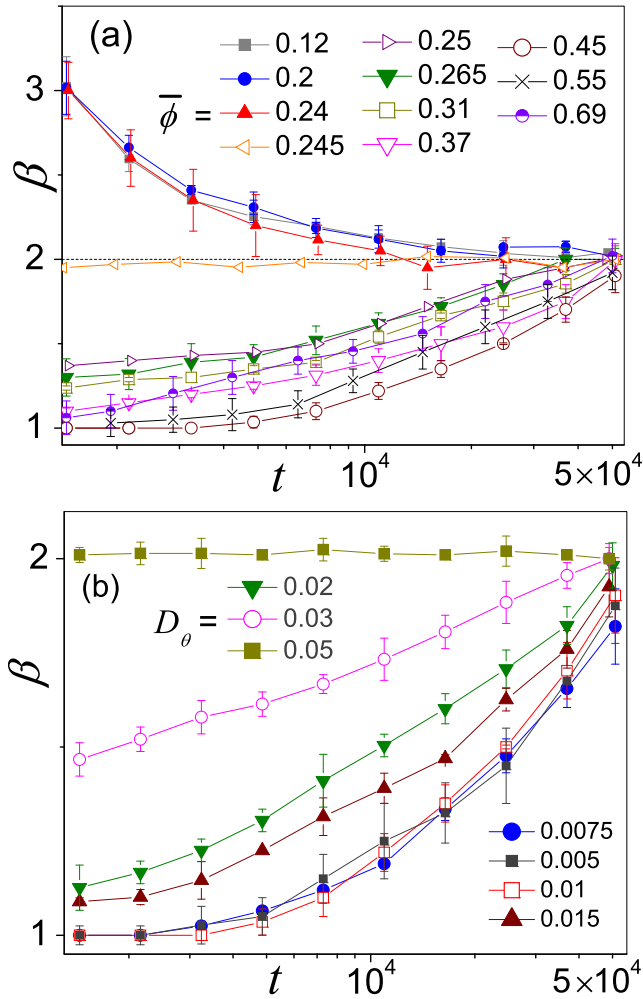


FIG. 5. Non-Gaussian normal diffusion as a MIPS signature. (a) NGND parameter β vs t for increasing values of $\bar{\phi}$. Phase coexistence is clearly characterized by leptokurtic transient $P(\Delta x, t)$ with fat tails ($\beta < 2$). (b) β vs t with $\bar{\phi} = 0.45$ and increasing D_θ (see legends). All simulations were performed assuming a randomly uniform initial particle distribution. Other simulation parameters are: $\tau_\theta = 100$, $v_0 = 1$, and $N = 9120$. The estimated NGND transient time is $\tau_{\text{NGND}} \sim 7.5 \times 10^5$ (see text).

of different sizes. Due to simultaneous multiple collisions, the instantaneous particle diffusion in such aggregates is Gaussian, with diffusion constant in the range $[0, D_s]$. As discussed in Ref. [20], correlations of the instantaneous diffusion constant on a suitably long timescale suffice to produce leptokurtic profiles of $P(\Delta x, t)$ with $1 < \beta < 2$. Here, such correlations are related to the ultraslow particle diffusion in the dense phase [28].

B. In-cluster diffusion constant and non-Gaussian normal diffusion transient time

The NGND mechanism assumes that the suspension has reached a (quasi)stationary state characterized by a normal average MSD. In view of the ergodic property, the particle diffusivity was averaged over the entire suspension, with the corresponding self-diffusion constant D of Fig. 1(b) making no difference between diffusion in the dilute phase and in the

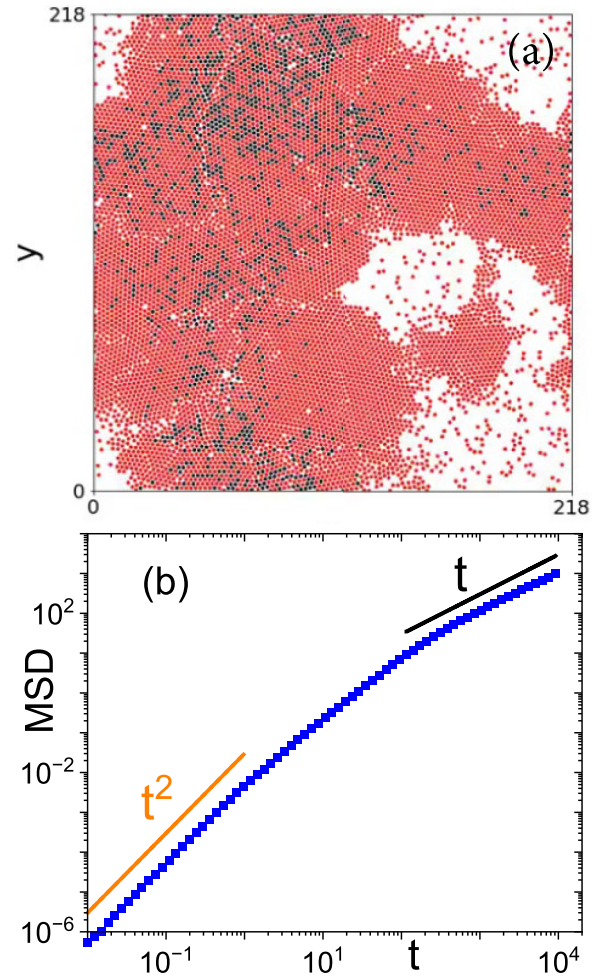


FIG. 6. In-cluster diffusion in a suspension of $N = 9120$ active JP's with $\bar{\phi} = 0.60$. All remaining simulation parameters are as in Fig. 1. (a) Randomly selected particles (black dots) inside the steady-state dense phase at $t = 10^4$; (b) MSD vs t of the selected particles diffusing along the x axis without leaving the dense phase. The corresponding asymptotic in-cluster diffusion constant, $D_c \sim 10^{-3} D_s$.

dense phase. The structure of the dense phase, in particular, is far from homogeneous [28] and keeps varying slowly with time. As a consequence, the diffusion of a single particle may appear normal over relatively short time intervals, but is in fact time modulated on longer timescales. To this purpose, we numerically estimated the asymptotic in-cluster diffusion constant D_c by monitoring the spatial diffusion of a number of particles randomly selected inside a steady-state cluster with $\bar{\phi} > \bar{\phi}_*$. Only trajectories of particles not leaving the cluster during the entire simulation run were averaged to compute the in-cluster MSD versus t (an example is displayed in Fig. 6). The resulting diffusion constant, $D_c \sim 10^{-3} D_s$, weakly depends on $\bar{\phi}$ and defines a characteristic NGND transient time, $\tau_{\text{NGND}} \sim \alpha_c L^2 / 8 D_c$ ($\alpha_c^{1/2} L$ being the average cluster diameter), in good agreement with the numerical data of Fig. 5.

VI. CONCLUSION

We characterized MIPS of an athermal, achiral active suspension by looking at the particle diffusivity under

steady-state conditions. The choice of using the overall suspension packing fraction as tunable parameter has a practical motivation, as in most applications the particle motility cannot be varied at will, while their density can. Particle diffusion under phase separation has been proven to show hysteretic and NGND properties. Our main conclusions are

(1) The hysteresis loop of the curve $D(\phi)$ in the lower binodal region, which allows a direct measure of ϕ_g and $\phi_g^{(s)}$.

(2) The peculiar properties of the upper binodal and spinodal curves, which appear to overlap, thus suppressing hysteresis in the upper binodal region. Our numerical data also suggest a mirror symmetry of the spinodal curves with $\phi_g^{(s)} + \phi_c^{(s)} = 1$.

(3) Non-Gaussian normal diffusion characterized motility induced phase separation with leptokurtic transient distributions of displacements Δx . The associated NGND transient time is almost four orders of magnitude larger than the ro-

tational relaxation time of a free JP. Further, we show that NGND characterized MIPS also in the presence of hysteresis.

ACKNOWLEDGMENTS

Y.L. is supported by NSF China under Grant No. 12375037, and F.M. is supported by NSF China under Grant No. 12350710786. P.K.G. is supported by SERB Core Research Grant No. CRG/2021/007394. P.B. thanks UGC, New Delhi, India, for the support via a Junior Research Fellowship. We thank the RIKEN supercomputer Hokusai for providing computational resources. F.N. is supported in part by the Japan Science and Technology Agency (JST) [via the CREST Quantum Frontiers program Grant No. JPMJCR24I2, the Quantum Leap Flagship Program (Q-LEAP), and the Moonshot R&D Grant No. JPMJMS2061], and the Office of Naval Research (ONR) Global (via Grant No. N62909-23-1-2074).

-
- [1] B. Wang, S. M. Anthony, S. C. Bae, and S. Granick, Anomalous yet Brownian, *Proc. Natl. Acad. Sci. USA* **106**, 15160 (2009).
- [2] B. Wang, J. Kuo, C. Bae, and S. Granick, When Brownian diffusion is not Gaussian, *Nat. Mater.* **11**, 481 (2012).
- [3] G. Kwon, B. J. Sung, and A. Yethiraj, Dynamics in crowded environments: Is non-Gaussian Brownian diffusion normal? *J. Phys. Chem. B* **118**, 8128 (2014).
- [4] J. Guan, B. Wang, and S. Granick, Even hard-sphere colloidal suspensions display Fickian yet non-Gaussian diffusion, *ACS Nano* **8**, 3331 (2014).
- [5] C. Gardiner, *Stochastic Methods: A Handbook for the Natural and Social Sciences* (Springer, Berlin, 2009).
- [6] J. Kim, C. Kim, and B. J. Sung, Simulation study of seemingly Fickian but heterogeneous dynamics of two dimensional colloids, *Phys. Rev. Lett.* **110**, 047801 (2013).
- [7] S. Bhattacharya, D. K. Sharma, S. Saurabh, S. De, A. Sain, A. Nandi, and A. Chowdhury, Plasticization of poly(vinylpyrrolidone) thin films under ambient humidity: Insight from single-molecule tracer diffusion dynamics, *J. Phys. Chem. B* **117**, 7771 (2013).
- [8] W. He, H. Song, Y. Su, L. Geng, B. J. Ackerson, H. B. Peng, and P. Tong, Dynamic heterogeneity and non-Gaussian statistics for acetylcholine receptors on live cell membrane, *Nat. Commun.* **7**, 11701 (2016).
- [9] R. Jain and K. L. Sebastian, Diffusion in a crowded, rearranging environment, *J. Phys. Chem. B* **120**, 3988 (2016).
- [10] S. K. Ghosh, A. G. Cherstvy, D. S. Grebenkov, and R. Metzler, Anomalous, non-Gaussian tracer diffusion in crowded two-dimensional environments, *New J. Phys.* **18**, 013027 (2016).
- [11] E. Lemaître, I. M. Sokolov, R. Metzler, and A. V. Chechkin, Non-Gaussian displacement distributions in models of heterogeneous active particle dynamics, *New J. Phys.* **25**, 013010 (2023).
- [12] S. M. J. Khadem, N. H. Siboni, and S. H. L. Klapp, Transport and phase separation of active Brownian particles in fluctuating environments, *Phys. Rev. E* **104**, 064615 (2021).
- [13] D. Debnath, P. K. Ghosh, V. R. Misko, Y. Li, F. Marchesoni, and F. Nori, Enhanced motility in a binary mixture of active nano/microswimmers, *Nanoscale* **12**, 9717 (2020).
- [14] M. V. Chubynsky and G. W. Slater, Diffusing diffusivity: A model for anomalous, yet Brownian, diffusion, *Phys. Rev. Lett.* **113**, 098302 (2014).
- [15] A. G. Cherstvy and R. Metzler, Anomalous diffusion in time-fluctuating non-stationary diffusivity landscapes, *Phys. Chem. Chem. Phys.* **18**, 23840 (2016).
- [16] R. Jain and K. L. Sebastian, Diffusing diffusivity: A new derivation and comparison with simulations, *J. Chem. Sci.* **129**, 929 (2017).
- [17] N. Tyagi and B. J. Cherayil, Non-Gaussian Brownian diffusion in dynamically disordered thermal environments, *J. Phys. Chem. B* **121**, 7204 (2017).
- [18] A. V. Chechkin, F. Seno, R. Metzler, and I. M. Sokolov, Brownian yet non-Gaussian diffusion: From superstatistics to subordination of diffusing diffusivities, *Phys. Rev. X* **7**, 021002 (2017).
- [19] Y. Li, F. Marchesoni, D. Debnath, and P. K. Ghosh, Non-Gaussian normal diffusion in a fluctuating corrugated channel, *Phys. Rev. Res.* **1**, 033003 (2019).
- [20] Q. Yin, Y. Li, F. Marchesoni, S. Nayak, and P. K. Ghosh, Non-Gaussian normal diffusion in low dimensional systems, *Front. Phys.* **16**, 33203 (2021).
- [21] *Janus Particle Synthesis, Self-Assembly and Applications*, edited by S. Jiang and S. Granick (RSC Publishing, Cambridge, 2012).
- [22] A. Walther and A. H. E. Müller, Janus particles: Synthesis, self-assembly, physical properties, and applications, *Chem. Rev.* **113**, 5194 (2013).
- [23] M. C. Marchetti, J. F. Joanny, S. Ramaswamy, T. B. Liverpool, J. Prost, M. Rao, and R. A. Simha, Hydrodynamics of soft active matter, *Rev. Mod. Phys.* **85**, 1143 (2013).
- [24] J. Elgeti, R. G. Winkler, and G. Gompper, Physics of microswimmers, single particle motion and collective behavior: a review, *Rep. Prog. Phys.* **78**, 056601 (2015).
- [25] S. Sengupta, M. E. Ibele, and A. Sen, Fantastic voyage: Designing self-powered nanorobots, *Angew. Chem. Int. Ed.* **51**, 8434 (2012).
- [26] J. Wang, *Nanomachines: Fundamentals and Applications* (Wiley-VCH, Weinheim, 2013).

- [27] Y. Fily and M. C. Marchetti, Athermal phase separation of self-propelled particles with no alignment, *Phys. Rev. Lett.* **108**, 235702 (2012).
- [28] G. S. Redner, M. F. Hagan, and A. Baskaran, Structure and dynamics of a phase-separating active colloidal fluid, *Phys. Rev. Lett.* **110**, 055701 (2013).
- [29] G. S. Redner, C. G. Wagner, A. Baskaran, and M. F. Hagan, Classical nucleation theory description of active colloid assembly, *Phys. Rev. Lett.* **117**, 148002 (2016).
- [30] See, for a recent review, J. O’Byrne, A. Solon, J. Tailleur, and Y. Zhao, in *Out-of-equilibrium Soft Matter*, edited by C. Kurzthaler, L. Gentile, and H. A. Stone (The Royal Society of Chemistry, London, 2023), Chap. 4, pp. 107–150.
- [31] A. K. Omar, H. Row, S. A. Mallory, and J. F. Brady, Mechanical theory of nonequilibrium coexistence and motility-induced phase separation, *Proc. Natl. Acad. Sci. USA* **120**, e2219900120 (2023).
- [32] M. E. Cates and C. Nardini, Classical nucleation theory for active fluid phase separation, *Phys. Rev. Lett.* **130**, 098203 (2023).
- [33] A. P. Solon, J. Stenhammar, M. E. Cates, Y. Kafri, and J. Tailleur, Generalized thermodynamics of motility-induced phase separation: Phase equilibria, laplace pressure, and change of ensembles, *New J. Phys.* **20**, 075001 (2018).
- [34] J. Bialké, T. Speck, and H. Löwen, Crystallization in a dense suspension of self-propelled particles, *Phys. Rev. Lett.* **108**, 168301 (2012).
- [35] F. Turci and N. B. Wilding, Phase separation and multibody effects in three-dimensional active Brownian particles, *Phys. Rev. Lett.* **126**, 038002 (2021).
- [36] A. K. Omar, K. Klymko, T. GrandPre, and P. L. Geissler, Phase diagram of active Brownian spheres: Crystallization and the metastability of motility-induced phase separation, *Phys. Rev. Lett.* **126**, 188002 (2021).
- [37] P. K. Ghosh, V. R. Misko, F. Marchesoni, and F. Nori, Self-propelled Janus particles in a ratchet: Numerical simulations, *Phys. Rev. Lett.* **110**, 268301 (2013).
- [38] P. Bag, S. Nayak, T. Debnath, and P. K. Ghosh, Directed autonomous motion and chiral separation of self-propelled Janus particles in convection roll arrays, *J. Phys. Chem. Lett.* **13**, 11413 (2022).
- [39] J. D. Weeks, D. Chandler, and H. C. Andersen, Role of repulsive forces in determining the equilibrium structure of simple liquids, *J. Chem. Phys.* **54**, 5237 (1971).
- [40] X. Yang, C. Liu, Y. Li, F. Marchesoni, P. Hänggi, and H. P. Zhang, Hydrodynamic and entropic effects on colloidal diffusion in corrugated channels, *Proc. Natl. Acad. Sci. USA* **114**, 9564 (2017).
- [41] P. E. Kloeden and E. Platen, *Numerical Solution of Stochastic Differential Equations* (Springer, Berlin, 1992).
- [42] R. Soto, M. Pinto, and R. Brito, Kinetic theory of motility induced phase separation for active Brownian particles, *Phys. Rev. Lett.* **132**, 208301 (2024).
- [43] P. Digregorio, D. Levis, A. Suma, L. F. Cugliandolo, G. Gonnella, and I. Pagonabarraga, Full phase diagram of active Brownian disks: From melting to motility-induced phase separation, *Phys. Rev. Lett.* **121**, 098003 (2018).
- [44] J. U. Klamsner, S. C. Kapfer, and W. Krauth, Thermodynamic phases in two-dimensional active matter, *Nat. Commun.* **9**, 5045 (2018).
- [45] J. Su, M. Feng, Y. Du, H. Jiang, and Z. Hou, Motility-induced phase separation is reentrant, *Commun. Phys.* **6**, 58 (2023).
- [46] H. Risken, *The Fokker-Planck Equation* (Springer, Berlin, 1984), Chap. 11.